




Article

Dynamic Mechanical Behavior of the Frozen Red Sandstone under Coupling of Saturation and Impact Loading

Junce Xu ¹ , Hai Pu ^{1,2,*}  and Ziheng Sha ¹ 

¹ State Key Laboratory for Geomechanics and Deep Underground Engineering, China University of Mining and Technology, Xuzhou 221116, China; xujunce@cumt.edu.cn (J.X.); zhsha@cumt.edu.cn (Z.S.)

² College of Mining Engineering and Geology, Xinjiang Institute of Engineering, Urumqi 830091, China

* Correspondence: haipu@cumt.edu.cn

Abstract: Saturation is one of the critical factors causing frost damage to rock masses in alpine regions, and dynamic stress perturbations further complicate the damage process. Therefore, the effects of water content and loadings should be considered in the construction and maintenance of rock structures during winter in cold regions. In this study, the effects of saturation and impact loading on the dynamic mechanical behavior of frozen red sandstone were investigated using a low-temperature split Hopkinson pressure bar system (LT-SHPB). By combining low-field nuclear magnetic resonance (LF-NMR) and scanning electron microscopy (SEM), the dynamic evolution of the microstructure of the frozen sandstone due to changes in saturation was investigated. The results indicated that the increase of saturation reshapes the pore structure of the frozen sandstone and promotes the expansion of pores of different sizes during freezing, while at complete saturation the frozen samples are mainly developed with meso- and macropores. The dynamic strength, elastic modulus, and brittleness index of the frozen sandstone under impact loading, which are limited by the critical saturation S_{rc} , tend to increase and then decrease with saturation. For the four impact loads, the dynamic strength of the samples increased by 21.2%, 27.1%, 32.5%, and 34.3% when the saturation was increased from 0 to 50%, corresponding to 1.38, 1.43, 1.51, and 1.56 times the dynamic strength of the fully saturated samples, respectively. In contrast, the ultimate deformation capacity of the frozen sandstone showed an opposite trend with saturation. As the impact load increases, the dynamic strength, elastic modulus, and peak strain of the frozen sandstone show a significant strengthening effect due to the increase in strain rate, while its brittleness index gradually decreases, dropping by 11.2% at full saturation. In addition, the energy dissipation capacity of the frozen sample first increases and then decreases with increasing saturation, with the enhancement effect of saturation on energy dissipation smaller than the weakening effect.

Keywords: saturation; frozen sandstone; SHPB; dynamic mechanics; brittleness



Citation: Xu, J.; Pu, H.; Sha, Z. Dynamic Mechanical Behavior of the Frozen Red Sandstone under Coupling of Saturation and Impact Loading. *Appl. Sci.* **2022**, *12*, 7767. <https://doi.org/10.3390/app12157767>

Academic Editors: Zhengzhao Liang, Bei Jiang and Nuwen Xu

Received: 6 July 2022

Accepted: 1 August 2022

Published: 2 August 2022

Publisher's Note: MDPI stays neutral with regard to jurisdictional claims in published maps and institutional affiliations.



Copyright: © 2022 by the authors. Licensee MDPI, Basel, Switzerland. This article is an open access article distributed under the terms and conditions of the Creative Commons Attribution (CC BY) license (<https://creativecommons.org/licenses/by/4.0/>).

1. Introduction

Under the influence of surface runoff and groundwater migration or seepage, water is not evenly distributed in the rock mass, resulting in significant variations in saturation. At low temperatures ($<0\text{ }^{\circ}\text{C}$), the water in the pores turns into ice, resulting in a volume increase of approximately 9% and reshaping the pore structure [1,2]. As a result, there are differences in the mechanical responses of rocks with different saturations after freezing [3]. In addition, rock structures in cold regions often suffer from dynamic loading [4]. For example, rock slopes in open-pit mines are affected by frost damage and are also susceptible to blasting, leading to geological hazards on the slopes [5]. Therefore, a comprehensive understanding of the dynamic mechanical behavior of frozen rock with different saturation is essential for the safe operation of rock structures in cold regions.

The mechanical properties of frozen rock under static loading have been extensively studied. At low temperatures, the static mechanical properties of rocks, such as strength,

modulus, cohesion, and internal friction angle, are significantly improved [6,7]. The presence of pore ice is a key factor in improving the properties of rocks at low temperatures [8,9]. For example, dry rocks show little change in mechanical properties at low temperatures, while the properties of saturated rock (e.g., strength or modulus) show an increasing tendency, with the effect being exacerbated in colder environments [10,11]. Unlike other factors such as temperature, freezing time, etc., the mechanical response of rocks at low temperatures is closely related to saturation, and their mechanical properties are controlled by the coupling of water weakening and ice solidification. However, when saturation exceeds a critical value, the volume growth of pore ice leads to damage, which is manifested by a rapid increase in local strain and the number of internal microcracks [12]. By performing strain and acoustic emission tests on frozen sandstone with different saturations, Huang et al. [7] found that significant strain and acoustic emission signals were present during freezing only when the saturation exceeded 80%. However, current studies on the mechanical behavior of rock at low temperatures have mainly focused on saturated rock, especially under quasi-static loading, and may not fully reflect the mechanical behavior under dynamic loading.

The dynamic mechanical characteristics of rocks at low temperatures have attracted more attention with the increase in rock structures in cold regions [13,14]. The split Hopkinson pressure bar (SHPB) system is the main equipment for dynamic testing [15,16]. The SHPB test system has been used to investigate the dynamic mechanical properties and deformation behavior of rock under freeze–thaw action [17–19]. It was found that the dynamic strength and deformation resistance decreased with freeze–thaw cycles [20]. However, for some rock projects built in cold regions, the study of rock dynamics at low temperatures is of more practical importance than the cyclic freeze–thaw action [21]. For example, wet rocks in seismic- or blast-disturbed zones show softening effects under the coupling of low temperature and dynamic loading, which is the main source of geological hazards [22]. To this end, Chen et al. [5] conducted a series of SHPB tests on frozen saturated sandstones and concluded that the dynamic mechanical properties of saturated frozen rocks are significantly different from those of dry rocks due to pore ice. As noted by Weng et al. [23], saturation is a key factor affecting the dynamic strength of frozen rock. However, research on dynamic mechanical properties of the rock at low temperatures is limited and focuses mainly on dry or saturated conditions.

Therefore, samples with different saturations were prepared using red sandstone from Xinjiang, China, and impact tests were conducted using a LT-SHPB system. Based on the results, the effects of saturation on dynamic strength, deformation, brittleness, and energy conversion of the frozen sample were investigated. In addition, LT-NMR and SEM were used to investigate the changes in the microstructure of the samples. Finally, the effects of saturation on the microstructure and mechanical response of the sample were discussed.

2. Material and Methods

2.1. Material and Samples Preparation

The distribution of cold regions in China is shown in Figure 1. Xinjiang Province belongs to the shallow and medium-depth seasonal permafrost regions, which makes rock work in this region vulnerable to frost damage [4]. At the same time, the area is a base for open-pit coal mining in China, and winter workings are prone to landslides and other geological hazards [5]. Therefore, the red sandstone used for testing was obtained from an open-pit mine in Urumqi (Figure 1), which is structurally intact, uniformly granular, and brownish red in color. The primary mineral composition of the rock was determined by X-ray diffraction (XRD) (Figure 2), revealing that the sandstone is composed mainly of quartz (47.3%), feldspar (31.5%), and illite (9%), with minor amounts of calcite and chlorite.

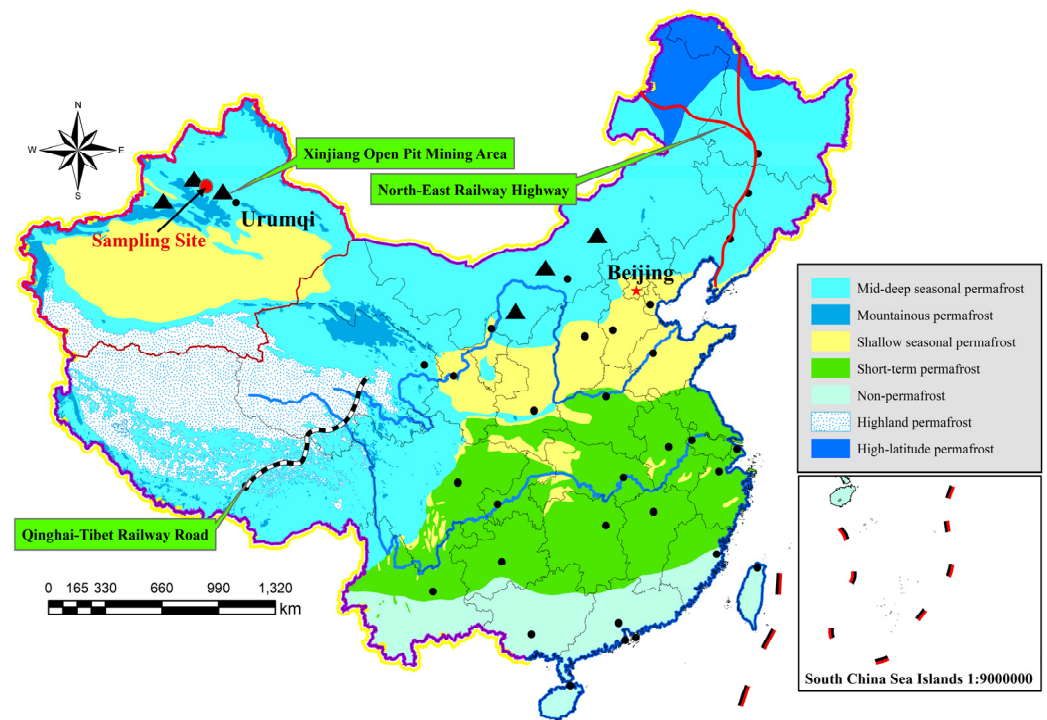


Figure 1. Distribution of cold regions in China and sampling points for the red sandstone sample; the red circles refer to the approximate locations of the sandstone sampling.

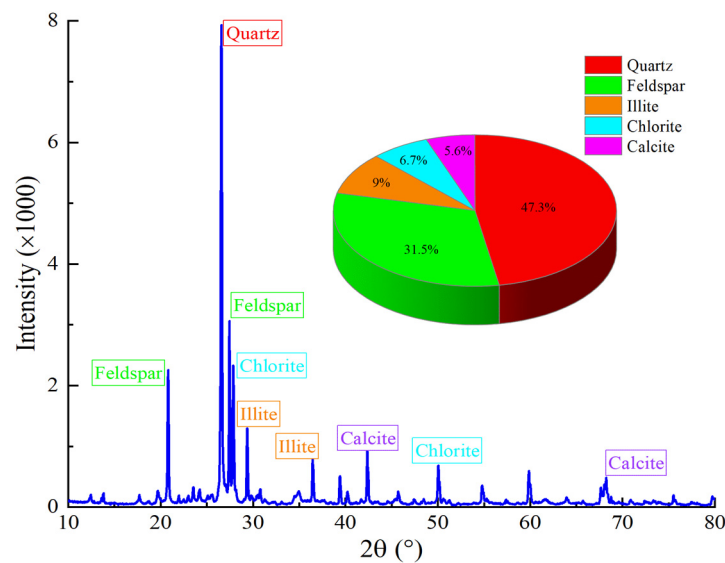


Figure 2. XRD result for the tested sandstone.

As shown in Figure 3, fresh red sandstone block was processed into standard samples with a diameter of 50 mm and a length-to-diameter ratio of 1 [24]. To reduce the influence of rock structure, all samples were taken from the same block and in the same direction. Moreover, both ends of the sample had to be ground to a tolerance of 0.02 mm, with no more than 0.1% rad from the perpendicular to the axis. Once the samples were machined, an ultrasonic detector was used to measure the P-wave velocity and select samples with similar P-wave velocity. In addition, five samples with a length and diameter of 50 × 100 mm were selected for physical and mechanical tests, with the results listed in Table 1.

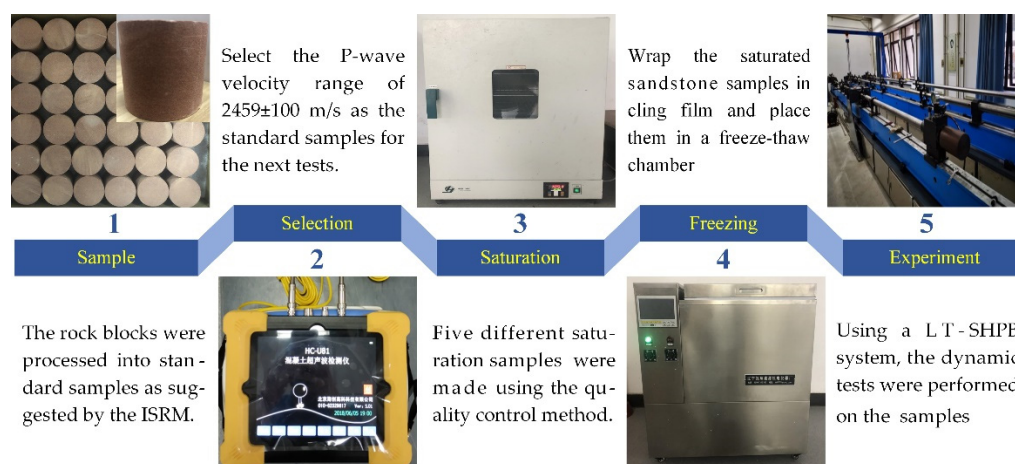


Figure 3. Experimental procedure and equipment.

Table 1. The physical and mechanical parameters of selected samples.

V_p (m/s)	ρ_d (g·cm ⁻³)	ρ_{sat} (g·cm ⁻³)	n (%)	σ_p (MPa)	η (%)
2459	2.14	2.31	16.57	13.84	7.94

Notes: V_p , P-wave velocity; ρ_d , dry density; ρ_{sat} , saturation density; n , porosity; σ_p , uniaxial compressive strength; η , water content.

To obtain the samples with different saturations (Figure 3), the selected samples were first dried in a drying oven at 105 °C for 48 h until their mass remained constant. The samples were then saturated with pure water for 24 h using a vacuum saturator. Thereafter, the samples were evaporated in a drying oven at 50 °C and weighed at intervals of 0.5 to 1 h to obtain the specified saturation [25]. The saturations for the test were set to dry (0%), 30%, 50%, 80%, and fully saturated (100%). Finally, considering the winter temperatures at the sampling site, the prepared samples were placed in a freeze–thaw chamber to freeze at −25 °C for 12 h [4]. Following the methods described above, frozen samples with different saturations were obtained for SHPB tests at low temperatures.

2.2. Experimental System

2.2.1. LT-NMR System

In this study, a LT-NMR analysis system developed by Suzhou Niumag Ltd. is used. The resonance frequency of the device is 12.8 MHz, while the main magnetic field strength is approximately 0.3 T. The transverse relaxation time T_2 can be tested with the CPMG pulse sequence. The samples were frozen at 0%, 30%, 50%, 80%, and 100% saturation in a freeze–thaw chamber at −25 °C for 24 h. After freezing, samples were placed in water at 20 °C for 24 h before LT-NMR testing [6].

2.2.2. LT-SHPB System

As shown in Figure 4, a LT-SHPB system developed by China University of Mining and Technology was adopted to conduct the impact tests. The system consists of five main components: an impact loading system, a compression bar system, a data acquisition system, a damping system, and a low-temperature freezing system. In the experimental system, the bars and the striker are made of high-strength Cr40 alloy steel with diameters, P-wave velocities, yield strengths, and elastic modulus of 50 mm, 5400 m/s, 800 MPa, and 208 GPa, respectively. The low-temperature freezing system consists of a temperature controller, a liquid nitrogen tank, an electric heating wire sensor, and a cold chamber. The cold chamber, as the key structure of the system, has a good insulating effect. Its inner insulation layer is mainly composed of aluminum silicate acupuncture blanket and insulating brick.

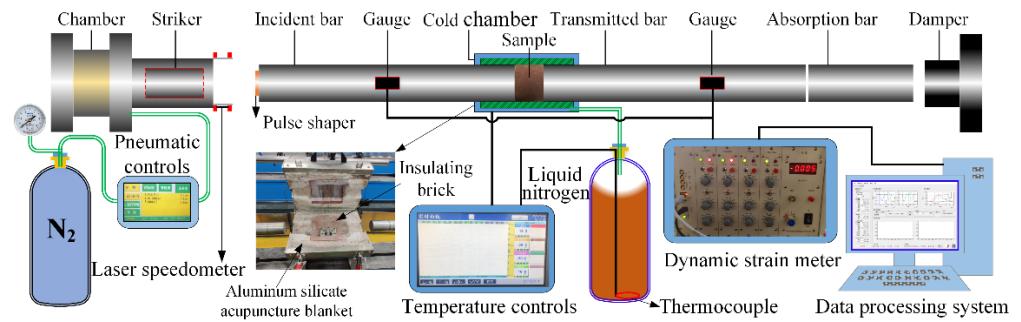


Figure 4. The LT-SHPB system.

Before the test, the chamber temperature was set to $-25\text{ }^{\circ}\text{C}$. The frozen sandstone sample was then quickly placed in the cold chamber. Molybdenum disulfide was applied at the ends as a lubricant to reduce the friction effect between the bars and the sample. It is worth mentioning that the sample should remain in the chamber for at least 0.5 h [5]. To obtain the desired waveform, a circular rubber pad with a diameter of 15 mm and a thickness of 2 mm was used as a pulse shaper. A compressive wave was generated when the high-pressure gas propelled the striker against the incident bar. Part of the compressive wave propagated through the sample to the transmission bar. As a result, the strain signal generated on the bar was measured by the strain gauges, as shown in Figure 5. Based on the one-dimensional stress wave propagation theory, the three-wave analysis method was used to calculate the strain and stress [26], as shown in Equation (1).

$$\begin{cases} \sigma = \frac{A_r E_0}{2} [\varepsilon_i(t) + \varepsilon_r(t) + \varepsilon_t(t)] \\ \varepsilon = \frac{C_s}{L_s} \int_0^t [\varepsilon_i(t) - \varepsilon_r(t) - \varepsilon_t(t)] dt \\ \dot{\varepsilon} = \frac{C_s}{L_s} [\varepsilon_i(t) - \varepsilon_r(t) - \varepsilon_t(t)] \end{cases} \quad (1)$$

where σ , ε , and $\dot{\varepsilon}$ refer to dynamic stress, dynamic stress, and strain rate, respectively; A_r is the ratio of the cross-sectional area of the bar to the sample; E_0 , C_s , and L_s are the elastic modulus, the wave velocity of the bar, and the length of the sample, respectively; $\varepsilon_i(t)$, $\varepsilon_r(t)$, and $\varepsilon_t(t)$ refer to the incident, reflected, and transmitted strain, respectively. In addition, the striker impact velocity is measured by a laser beam measurement system.

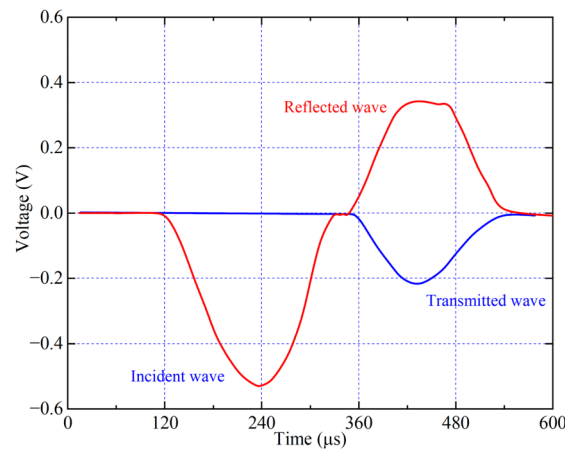


Figure 5. Typical strain gauge signals.

2.3. Dynamical Testing Scheme

As mentioned earlier, samples with five different saturations were selected for the impact tests. Four test groups were designed using impact velocity as the loading condition:

4 m/s, 5 m/s, 6 m/s, and 7 m/s. Each group contains three samples. As a result, 60 samples were required to carry out the tests, with five additional samples prepared as spares. For simplicity, the samples were numbered, e.g., D-80-7 denotes the frozen samples at 80% saturation with an impact velocity of 7 m/s at low temperatures. Moreover, the uniformity of the stress at both ends of the samples must be verified before performing the dynamic tests. As shown in Figure 6, the superposition of incident and reflected waves largely coincides with the transmitted waves, which means that the stresses at both ends of the sample are in equilibrium during loading [24].

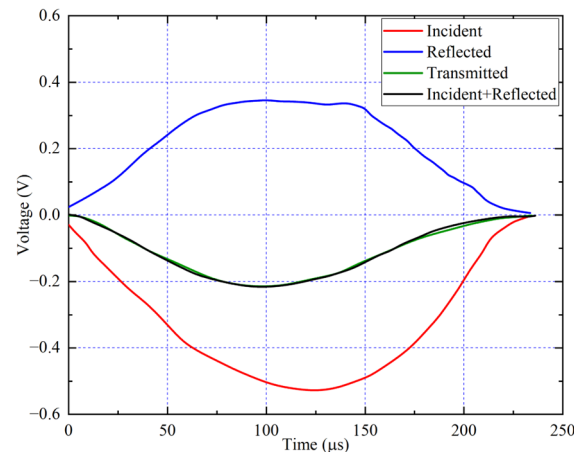


Figure 6. Verification of test stress uniformity hypothesis.

3. Experimental Results and Analysis

3.1. LT-NMR Results

Low-field NMR tests were performed on the samples to investigate the effect of water content on the microstructure at low temperatures. In the NMR study, the intensity of the magnetic resonance signal (MR) represents the amount of hydrogen-containing liquid in the sample, while the change rate of the MR signal over time (relaxation time T_2) is related to the state of the molecules in the liquid. Therefore, analyzing the relaxation time of the hydrogen-containing liquid could provide a comprehensive view of the pore space distribution in the rock [27]. For a hydrogen-containing fluid (water) in the rock, the transverse relaxation time T_2 is:

$$\frac{1}{T_2} = \rho \left(\frac{S}{V} \right)_{\text{pore}} \quad (2)$$

where T_2 is the transverse relaxation time (ms); ρ indicates the surface relaxation strength, which is related to the surface of the rock particles and the nature of the cement [13]; and S/V refers to the specific surface of the pores in the rock, which is related to the shape of the pore, e.g., if the pore is spherical, it is taken as $3/R$. Therefore, observing the characteristics of the T_2 spectrum of the sample can indirectly obtain the distribution pattern of different pore sizes.

The distribution curves of the T_2 spectrum of the sandstone samples for 0%, 30%, 50%, 80%, and 100% are shown in Figure 7. The T_2 spectrum distribution mainly has three peaks, indicating that three sizes of pore structures were mainly formed in the sample. Moreover, the area under the peaks is mainly between 0.1~10 ms. According to Yao et al. [28], there is a correlation between T_2 , pore diameter, and water type. For example, when T_2 is 10~100 ms, the pore size is 0.1~1 μm and is called mesopore, which is mainly composed of capillary water [27]. As shown in Figure 7, for the dried sample, the area of the T_2 spectrum per size decreases compared to other saturated samples. As saturation increases, the area occupied by the second peak gradually increases from 2.19% (dry) to 9.32% (100%), showing that the increase in saturation has a significant effect on the development of mesopores in the sample. When the saturation exceeds 80%, the area of the third peak

increases by 3.57%, indicating that the macropores of the sample have developed further. Thus, saturation has a strong influence on the pore development of the sample at low temperatures. When the saturation is less than 80%, the micropores and mesopores in the sample spread predominantly, while the macropores of the sample gradually develop when the saturation is greater than 80%. In other words, the higher the water content, the more significant the increase in porosity of the sample after freezing. This indicates that the increasing moisture accelerates the expansion of the pores inside the sample and increases the sensitivity of the sample to the freeze heave forces.

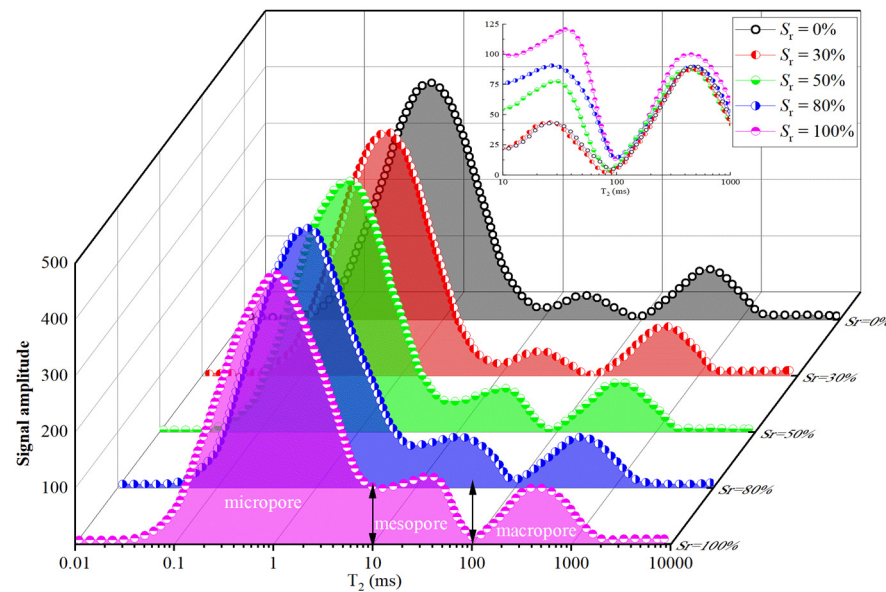


Figure 7. Distribution of the T_2 spectrum of the samples with different saturations.

3.2. Dynamic Impact Test Results

3.2.1. Dynamic Stress–Strain Behavior

In this study, four impact velocities were determined by adjusting N_2 pressure and the position of the striker [15]. The dynamic stress–strain curves of the sample with different saturations are shown in Figure 8a–e, while Figure 8f presents a typical stress–strain curve of the sample. The stress–strain behavior of frozen sandstone at low temperature has four stages, as shown in Figure 8f: (I) the initial compression stage, in which defects such as pores or microcracks in the sandstone gradually close under the action of compressive stress waves; (II) the linear elastic stage, in which elastic energy is rapidly accumulated; (III) the plastic deformation stage, in which defects such as microcracks in the sandstone begin to develop rapidly, characterized by a rapid increase in strain and a slow increase in stress; the initial and final points of the plastic stage are the yield point and the peak point of the sample with coordinates (σ_e, ϵ_e) and (σ_p, ϵ_p) ; and (IV) the post-peak stage, which is rarely mentioned because the samples are detached from the compression bars during this stage [5].

As can be seen in Figure 8, the stress–strain curves of the dried specimen show a distinct compression stage and decrease with the increasing impact velocity. Since the pore water freezes into ice with some bearing capacity at low temperatures, stage I gradually decreases with increasing saturation. For example, the curves show no compaction process when the saturation reaches 50%. On the other hand, thermal shrinkage of some mineral particles reduces the defect volume, thus reducing the initial damage. Moreover, the plastic stage III is closely related to saturation and impact velocity, which first decreases and then increases with increasing saturation. According to Equation (1), the dynamic stress versus time is shown in Figure 9. As the impact velocity increases, the plastic deformation occurs earlier, which is consistent with the results of Xing et al. [29]. In addition, the time of plastic

deformation first increases and then decreases with increasing saturation. Moreover, the time to reach the dynamic stress peak is negatively correlated with the impact velocity, while it is positively correlated with the impact strength. To clearly describe the changes in dynamic behavior, several parameters, namely peak strength, elastic modulus, and brittleness index (BI), were used to assess the effects of saturation and impact loading on the dynamic mechanical properties of the frozen sample. The results are listed in Table 2.

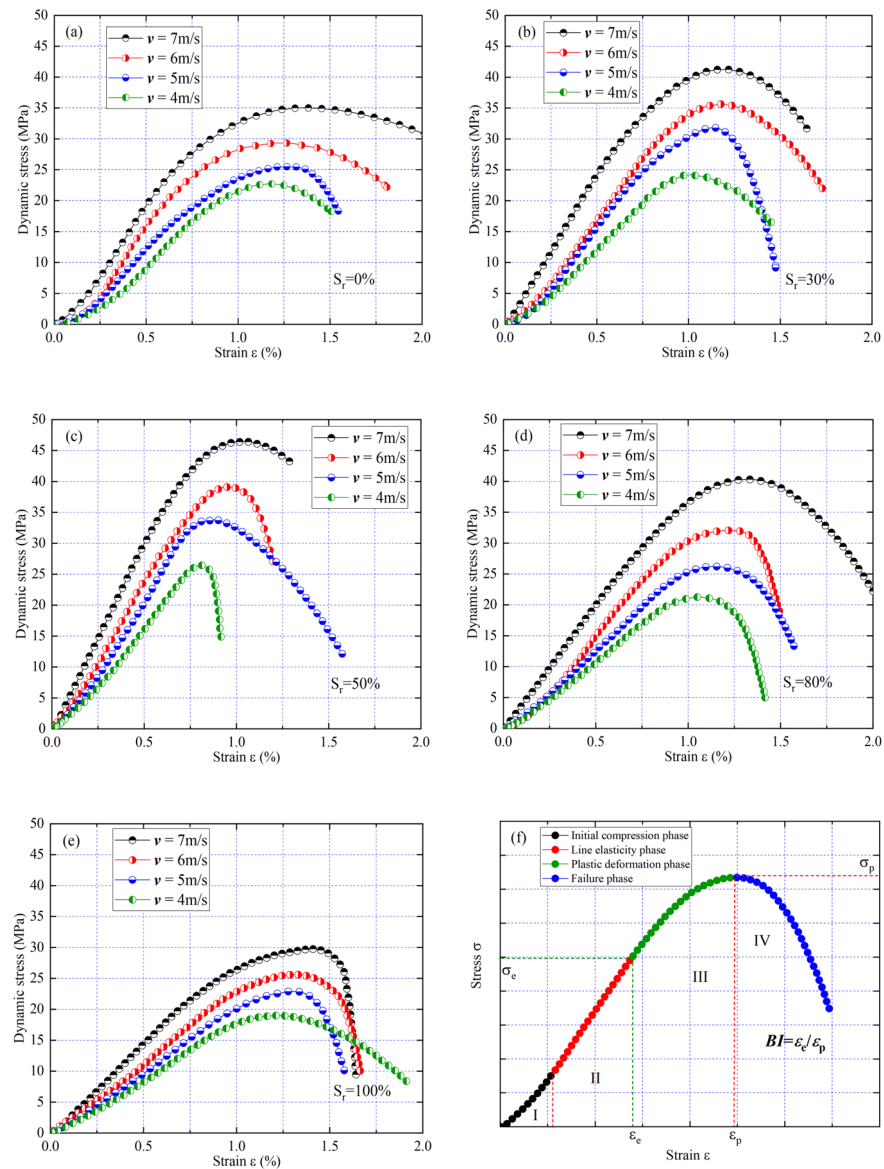


Figure 8. Dynamic stress–strain curves of the sample at low temperatures: (a–e) denote samples with saturation of 0%, 30%, 50%, 80%, and 100%, respectively; (f) shows the deformation phase divisions of typical stress–strain curves.

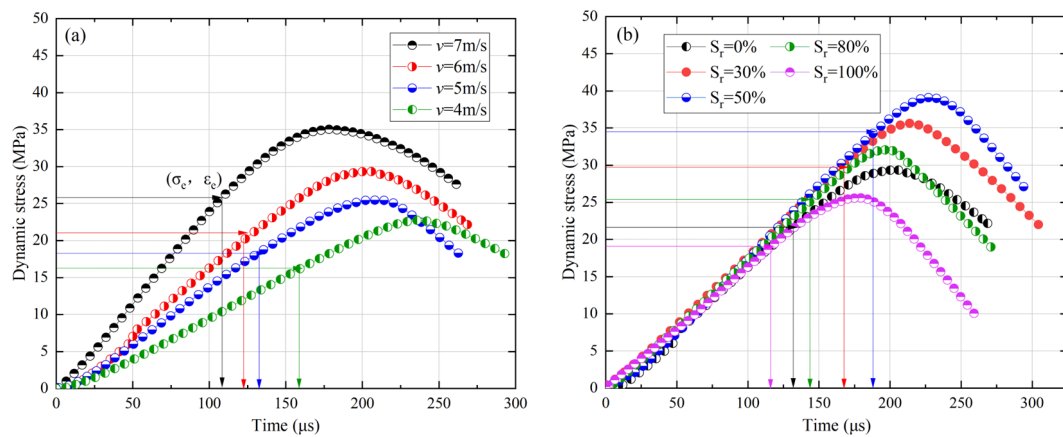


Figure 9. Dynamic stress versus time for frozen samples: (a) $S_r = 0\%$; (b) $v = 6$ m/s.

Table 2. Dynamic mechanical parameters of sandstone under different conditions.

Samples	Impact Velocity (m/s)	Dynamic Strength (MPa)	Dynamic Modulus (GPa)	Peak Strain (%)	Brittleness Index
D-0-4	4	22.1	1.95	1.167	0.728
D-0-5	5	25.7	2.04	1.247	0.694
D-0-6	6	29.3	2.28	1.286	0.657
D-0-7	7	34.6	2.59	1.353	0.602
D-30-4	4	24.6	2.39	1.015	0.753
D-30-5	5	31.3	2.83	1.094	0.721
D-30-6	6	35.5	3.03	1.176	0.697
D-30-7	7	42.8	3.42	1.218	0.665
D-50-4	4	26.4	3.26	0.812	0.862
D-50-5	5	33.8	3.8	0.891	0.819
D-50-6	6	39.7	4.07	0.961	0.760
D-50-7	7	46.5	4.47	1.041	0.682
D-80-4	4	21.3	2.02	1.049	0.788
D-80-5	5	26.2	2.27	1.154	0.745
D-80-6	6	32.6	2.58	1.238	0.703
D-80-7	7	40.3	3.06	1.318	0.675
D-100-4	4	19.4	1.71	1.134	0.744
D-100-5	5	23.6	1.83	1.292	0.712
D-100-6	6	25.5	1.92	1.331	0.684
D-100-7	7	28.8	2.11	1.411	0.659

Dynamic Strength

According to the data obtained from Table 2, the relationship between dynamic strength as a function of impact velocity and saturation of the frozen sandstone is shown in Figure 10. The dynamic strength of the sample at low temperatures increases linearly with increasing impact velocity. For example, when the impact velocity increased from 4 m/s to 7 m/s, the dynamic strengths of the sample with different saturations increased by 1.53 (0%), 1.77 (30%), 1.74 (50%), 1.89 (80%), and 1.48 (100%) times, respectively. However, it can be seen in Figure 10b that the dynamic strength of the sample does not increase uniformly with saturation. The dynamic strength ($v = 5$ m/s) increased by 24.9%, 32.7%, 2.86%, and -7.31% when the saturation increased from 0 to 100%. This indicates that the enhancement effect of pore ice is gradually suppressed by frost damage when the saturation of red sandstone exceeds 80%. At the same time, the enhancement effect of the frozen samples is less than the weakening effect at low temperatures when the saturation increases from 0 to 100% (Figure 10b). In general, the dynamic strength of frozen rock at low temperatures still has the strain rate effect, but it increases and then decreases with saturation.

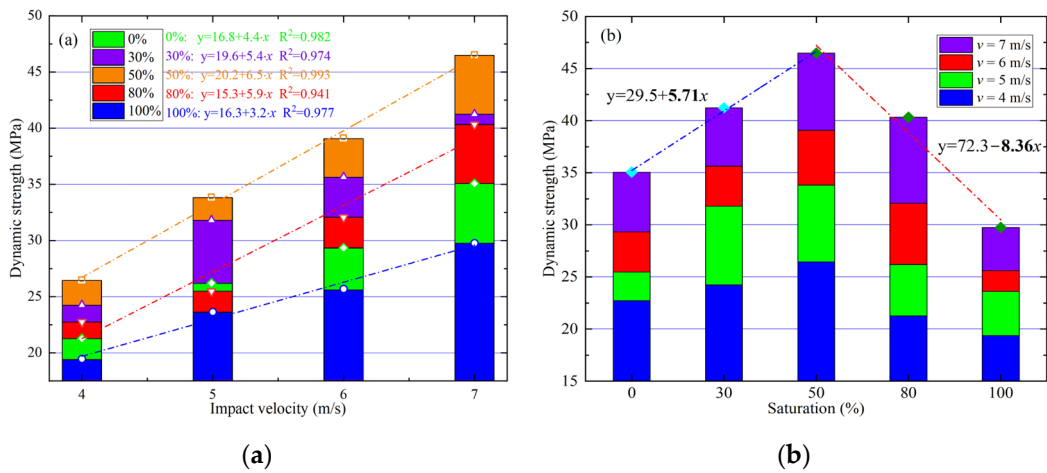


Figure 10. Dynamic peak strength versus impact velocity (a) and saturation (b) of the sample.

In addition, as shown in Figure 11, a dynamic strength increase factor (DIF) is introduced to evaluate the strength increase rate for the frozen samples. The DIF is determined using Equation (3), where $f_v(d)$ is the dynamic strength at the impact velocity v and $f(s)$ is the static strength [30]. From this, it can be seen that the DIF of the sample increases with increasing saturation and then decreases. For an impact velocity of 6 m/s, DIF increases from 2.11 to 2.87 as the saturation increases from 0 to 50%, while it decreases to 2.31 as saturation increases to 80%. As a result, it is reasonable to infer a critical saturation (S_{rc}) between 50% and 80% for the samples at low temperatures. When the saturation is greater than the critical saturation, the strength enhancement caused by the pore ice is gradually inhibited by the damage caused by the volume expansion. As the samples approach full saturation, the strength increase is further suppressed by the cracking and expansion of the pores under the action of the frost heave force.

$$DIF = \frac{f_v(d) - f(s)}{f(s)} \tag{3}$$

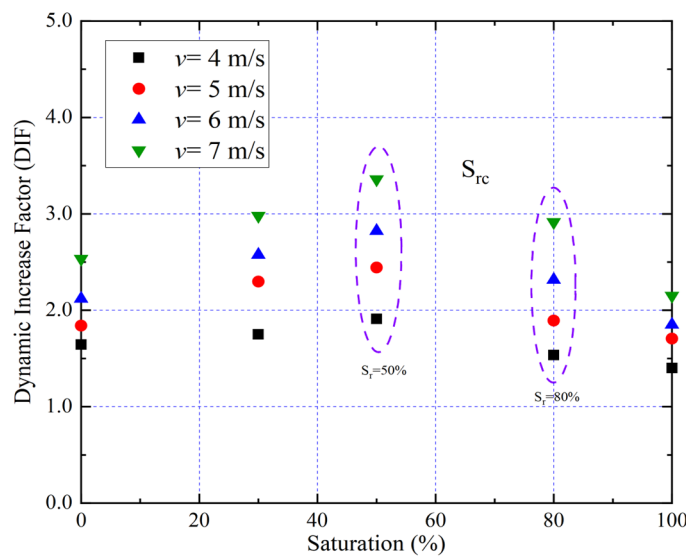


Figure 11. DIF versus impact velocity and saturation of the sample.

Indeed, the volume expansion (9%) caused by the pore ice exerts a frost heave force on the rock skeleton, thereby affecting cracking and expansion in the rock. Huang et al. [7]

found that the sample saturation is a crucial factor for controlling the frost heave force. The relationship between frost heave force P and saturation S_r is expressed in Equation (4) [31].

$$\begin{cases} P = \frac{[\beta n S_r u - n(1 - S_r)] K_r K_i}{K_r S_r + K_i} H[u - \chi] \\ H[u - \chi] = \begin{cases} 0 & (u \leq \chi) \\ 1 & (u > \chi) \end{cases} \\ \chi = \frac{1 - S_r}{\beta S_r} \end{cases} \quad (4)$$

where β is the volume expansion coefficient of ice; n represents the porosity; u denotes the freezing rate; K_r and K_i are the bulk modulus of the rock skeleton and the ice, respectively; and $H[u - \chi]$ is the step function. From Equation (4), the frost heave force is affected by the porosity, saturation, freezing rate, and bulk modulus of ice and rock skeleton. Here, β , K_r , and K_i are set to 0.09, 20.83 GPa, and 5 GPa, respectively [32]. The step function defaults to 1 and S_r values range from 0.8 to 1. Substituting the parameters into Equation (4) yields the relationship between frost heave stress, saturation, and freezing rate, which is shown in Figure 11.

As shown in Figure 12, the frost heave force is positively related to saturation; yet, even at 100% saturation, the effective heave force can still occur at lower freezing rates. As the freezing rate increases, the intensity factor of the frozen stress in the pore space exceeds the critical intensity factor K_{IC} , leading to the initiation and propagation of cracks and thus internal damage to the sample [33]. As a result, the dynamic strength of the sample increases and decreases with increasing saturation. However, due to the weak cementation of the rock in Xinjiang [34], the critical saturation of the red sandstone in the actual tests is between 50% and 80%, which is less than the predicted threshold of 91% for frost deformation failure.

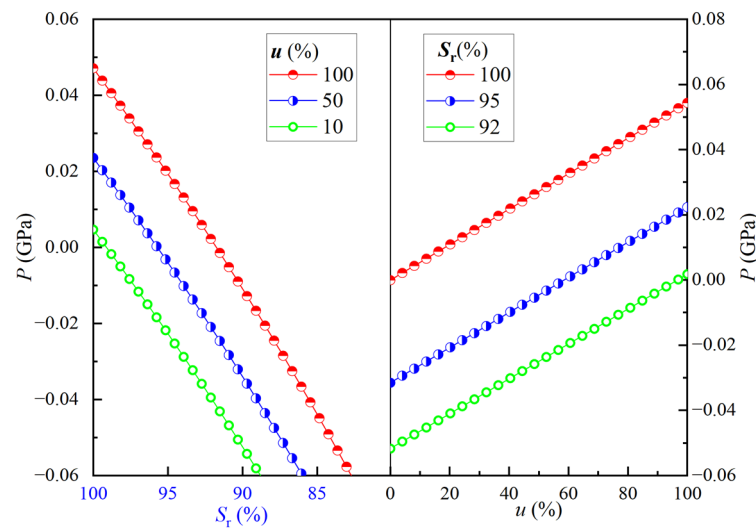


Figure 12. Frost heaving force versus saturation and freezing rates.

Dynamic Elastic Modulus

Following Figure 8f, the tangential modulus was adopted as the dynamic elastic modulus (E_d) in this study. The variation of E_d with impact velocity and saturation is shown in Figure 13. In Figure 13a, the E_d of the sample at low temperatures initially shows an increasing trend with saturation. For example, when the saturation of the sample increases from 0 to 50%, the E_d increases by 72.6% from 2.59 GPa to 4.47 GPa at an impact velocity of 7 m/s. However, as saturation increases (>50%), the increasing trend is suppressed and the E_d of the sample reduces by 18.5% to 2.11 GPa at complete saturation. The increase in deformation resistance is due to the pore ice acting as a support effect for the pore wall and enhancing the cementation between the wall and the ice, facilitating

the propagation of stress waves. As a result, the pore ice reduces the stress concentration at the pore tip [2], leading to an increase in dynamic modulus. However, as saturation increases, new microcracks appear in the sample under the influence of freeze heave forces and the enhancement of pore ice gradually decreases, leading to a decrease in dynamic elastic modulus. Moreover, as shown in Figure 13b, the E_d of the sample increases linearly with the impact velocity at low temperatures. Under the five saturation conditions, the E_d increases rapidly by 32.8 %, 43.1 %, 37.1 %, 51.5 %, and 23.4%, respectively, when the impact velocity increases from 4 m/s to 7 m/s, indicating that the stiffness property of the frozen sample has a significant impact on the strengthening effect.

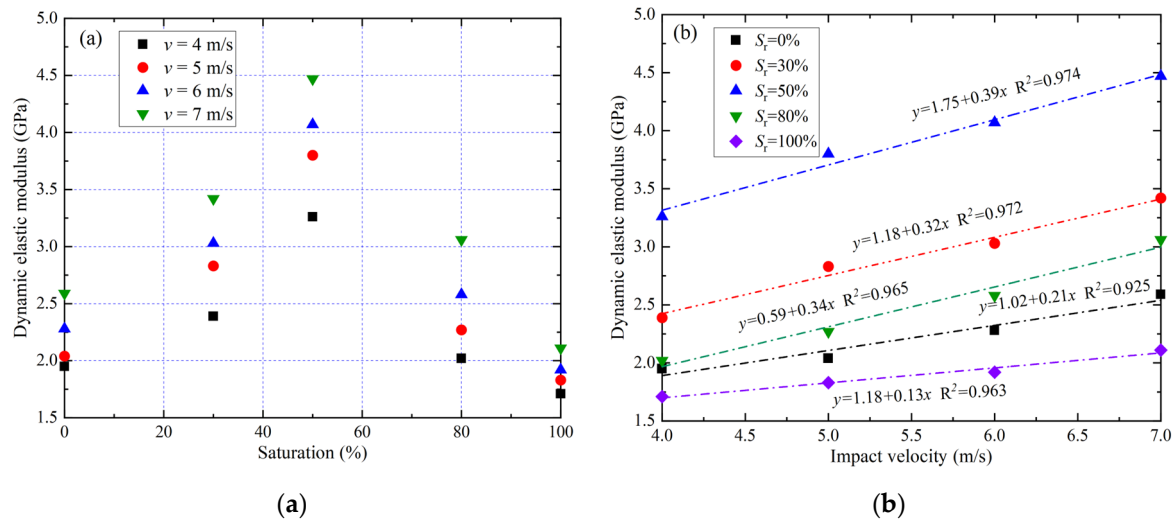


Figure 13. Dynamic elastic modulus versus saturation (a) and impact velocity (b) of the sample.

Dynamic Brittleness Index

Brittleness is an important parameter to describe the deformation and failure process of the rock [35]. Various external factors such as water content and temperature inevitably change the brittle state and failure pattern of rock [24]. Therefore, a brittleness index (BI) is used to characterize the effect of saturation on the pre-peak deformation characteristics of the frozen sample, as follows:

$$BI = \frac{\epsilon_e}{\epsilon_p} \tag{5}$$

where ϵ_e and ϵ_p refer to the yield point strain and peak point strain in the stress–strain curve, respectively. If BI has the value of 1, the sample is considered to be completely brittle, i.e., the larger the value of BI , the more brittle the sample is. From Table 2, the minimum value of BI is 0.602 and the maximum value is 0.862. The surface of BI for frozen sandstone as a function of initial saturation and impact velocity is shown in Figure 14.

As shown in Figure 14, the BI values of the sample decrease with increasing impact velocity, suggesting that impact velocity promotes the transition from very brittle to ductile frozen sandstone. Thus, BI values decrease by 17.4 %, 11.6 %, 20.9 %, 14.3 %, and 11.3 % at five saturation states, respectively, when the impact velocity is increased from 4 m/s to 7 m/s. In terms of energy, an increase in BI value means an increase in the elastic energy accumulation stage (II) and a decrease in the energy release stage (III) within the sample. Therefore, microcracks are less likely to propagate in the frozen sample at low impact velocities, consistent with the experimental results of Chen et al. [5]. In contrast, the BI value of the frozen sample tends to rise with increasing saturation due to pore ice. As a result, the stress–strain curves show a shortening in the stage (III) and an increase in the stage (II). However, when saturation exceeds critical saturation, pore ice plays a role in eliminating internal defects and drives crack propagation by frost heave forces. Therefore, two effects play a critical role in controlling the deformation behavior of the

frozen rock. For the tested rock, when the saturation is close to 80 %, the crack development within the sample under frost heave forces plays an important role. For example, when the saturation increases from 50 % to 80 %, the BI values decrease by 8.54 %, 9.04 %, 7.49 %, and 1.02 % at four impact velocities, respectively. Therefore, it can be inferred that the saturation distribution of the rock masses in the cold regions could affect the deformation characteristics under the impact loading.

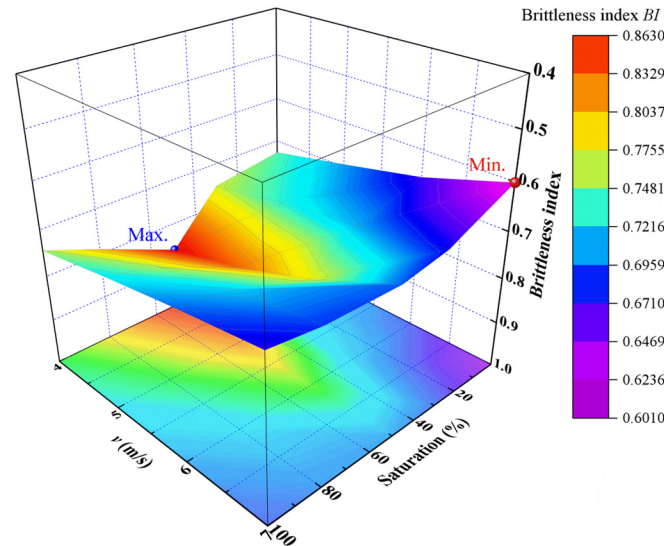


Figure 14. BI values versus impact velocity and saturation of the sample.

3.3. Energy Evolution

The failure of rock under impact loading can be considered as the result of the mutual transformation of the different forms of energy. During impact testing, the main forms of energy include the incident energy E_{in} , reflected energy E_{re} , transmitted energy E_{ti} , dissipated energy E_{di} , and other magnetic heat energy, with dissipated energy reflecting impact energy converted into fracture energy and other energy. From a microscopic point of view, energy dissipation reflects the continuous development of microdefects in the rock, while macroscopically it is represented as the gradual loss of rock strength. The energy evolution of the frozen sample under the impact load is calculated by Equation (6) [2], where A_s is the cross-sectional area of the incident bar.

$$\begin{cases} E_{in} = E_0 C_s A_s \int_0^t \varepsilon_1^2(t) dt \\ E_{re} = E_0 C_s A_s \int_0^t \varepsilon_r^2(t) dt \\ E_{tr} = E_0 C_s A_s \int_0^t \varepsilon_t^2(t) dt \\ E_{di} = E_{in} - (E_{re} + E_{tr}) \end{cases} \quad (6)$$

The energy conversion for frozen samples with different saturations is shown in Figure 15. As the impact velocity increases, all forms of energy show an increasing trend, with a quadratic polynomial accurately reflecting the changes. Moreover, the dissipated energy gradually overtakes the reflected energy as the saturation increases (Figure 15a). However, when the saturation increases above 50%, the reflected energy gradually increases faster than the dissipated energy (Figure 15b). This is due to the continuous increase in pore ice, which leads to a decrease in the wave impedance of the samples. To better assess the effect of saturation on the dissipated energy of the frozen sample, Equation (7) was used to calculate the dissipated energy per unit volume, η_d . The evolution of η_d with saturation for different impact velocities is shown in Figure 16. Taking 5 m/s as an example, η_d of the dried sample is 0.67 J/cm³ at low temperatures. As saturation increases, η_d begins to increase and reaches 0.76 J/cm³ and 0.82 J/cm³ at 30% and 50% saturation, corresponding

to an increase of 13.4 % and 22.4 %, respectively, over the dried sample. However, at 80 % and 100 % saturation, there is a significant decrease in η_d to 0.56 J/cm³ and 0.52 J/cm³, respectively. Therefore, it can be inferred that saturation has a considerable effect on the energy dissipation capacity of the frozen sample, where the range of 0~50% increases the energy dissipation capacity, while 50~100 % shows the effect of weakening. The effect of increasing the dissipated energy is less than the effect of weakening, indicating that the rock sample is sensitive to the work caused by the internal frost heave forces. In other words, when the saturation increases above 50 %, the frost heave forces promote the formation of more microcracks in the sample, which decreases the dissipated energy demand.

$$\eta_d = \frac{E_{di}}{V_s} \tag{7}$$

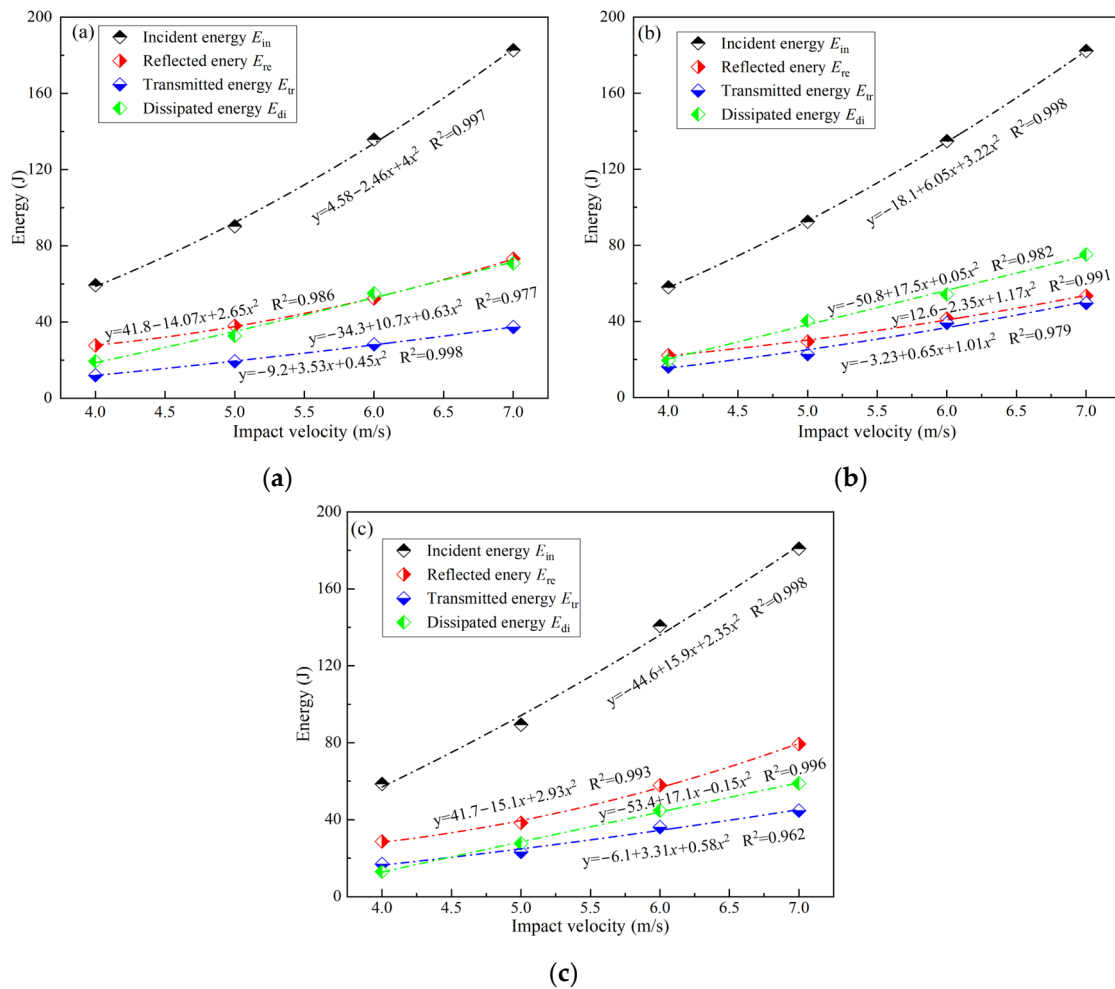


Figure 15. Evolution of rock energy distribution with saturation of (a) $S_r = 0\%$, (b) $S_r = 50\%$, and (c) $S_r = 100\%$.

3.4. Macro- and Microscopic Failure Features

The fracture behavior of rock is closely related to the impact velocity and microstructural changes during impact testing [36]. Hence, studying the fracture state during impact can show how saturation affects the mechanical properties of rock at low temperatures. After the tests, frozen sandstone fragments with different saturations were collected and dried. The results are presented in Table 3. It is obvious that the sandstone samples are completely broken at different impact velocities due to their relatively low strength. At low impact velocity (4 m/s), there were large broken blocks in the samples with different saturations, especially blocks approximately 5.9 cm in length in the sample with 50% saturation.

At this time, the pore ice within the sample played a role in supporting the pore wall and cementation, so that some of the crack development at the pore tip was suppressed under the action of the stress waves, reflecting the increase in the volume of macroscopically fractured blocks. Meanwhile, the plastic deformation before the peak during the impact test implies the development and extension of the internal microcracks, so the increase of plastic deformation indicates the increase of fragmentation degree. As can be seen in Figure 8, the plastic deformation increases with saturation and then decreases, which corresponds to the same trend in the fragmentation degree. Moreover, plastic deformation increases with the impact velocity, while the powder particles of the broken samples gradually increase in size. At an impact velocity of 7 m/s, the samples were broken into powder, indicating that the frozen sample mainly changed from tensile failure to complex fracture. Therefore, the final failure morphology of the samples can be used to infer the role of pore ice.

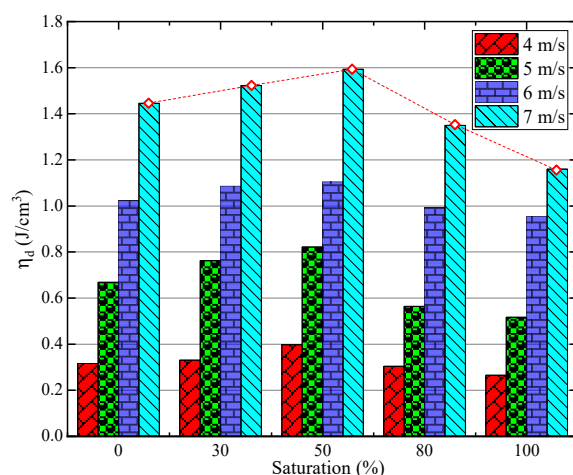


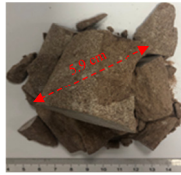







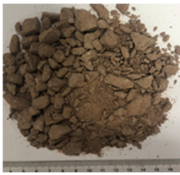
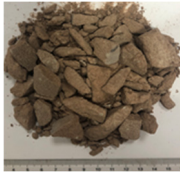


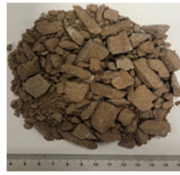
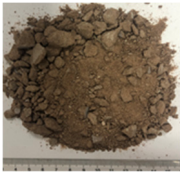
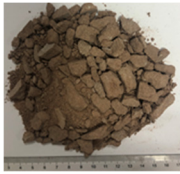


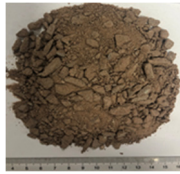


Figure 16. Dissipated energy per unit volume (η_d) of samples at low temperatures.

In addition, as shown in Figure 17, SEM images are used to infer changes in the microscopic morphology of the red sandstone after freezing. The images demonstrate that saturation has a significant effect on the surface morphology of the sample, and that many microcracks have formed after the freezing treatment. In the original state, the internal structure of the sandstone is relatively loose (Figure 17a) and has many small primary cracks, pores, and other defects, some of which can be up to 4 μm in width. After freezing, the surface structure becomes dense due to thermal contraction of the mineral particles, and some of the original cracks close, with a maximum crack width as small as 2 μm (Figure 17b). In Figure 17c, some of the previously closed cracks reactivate and propagate at low saturation as water freezes to ice at low temperatures. When the saturation increases to 50% (Figure 17d), some cracks develop further and connect, but most cracks are less than 1 μm in width, and the damaging effect of pore ice on the matrix is still less than its strengthening effect. However, when the sample saturation reaches 80%, the increasing pore water facilitates the continued expansion of the pore ice, leading to the development of larger cracks, some of which are up to 6 μm in width (Figure 17e). When the sample is fully saturated, a block appears on the fracture surface, indicating that the volume of ice expands even after the cracks are penetrated, causing the block to be extruded; meanwhile, the cracks on the fracture surface reach approximately 9 μm in width (Figure 17f). In summary, as the saturation increases, microcracks begin to develop inside the sample, while the strengthening of the pore ice prevents the manifestation of the internal damage to a certain extent. However, when the saturation exceeds 50%, the pores inside the sample cannot provide sufficient expansion space for the ice, resulting in a fracture network inside the sample. As a result, the strength and deformation resistance tend to decrease as the sample approaches full saturation.

Table 3. Impact failure modes of the frozen sample.

S_r	$S_r = 0\%$	$S_r = 30\%$	$S_r = 50\%$	$S_r = 80\%$	$S_r = 100\%$
Impact velocity 4 (m/s)					
Impact velocity 5 (m/s)					
Impact velocity 6 (m/s)					
Impact velocity 7 (m/s)					

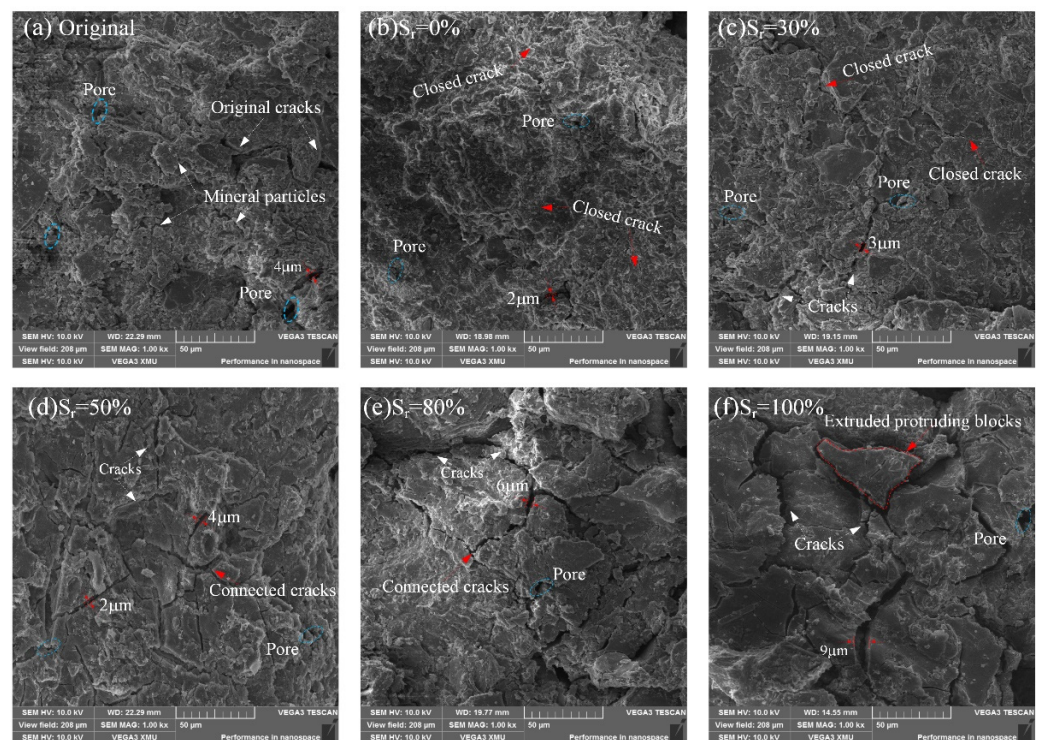


Figure 17. Microscopic characteristics of frozen sandstone sample with different saturation from SEM images (1000 \times).

4. Discussion

Due to groundwater migration and seepage, pore water in natural rock is not uniformly distributed, resulting in significant variations in rock saturation [3]. When the temperature drops below 0 °C, the pore water in the rock begins to freeze into ice. The pore ice remodels the pore structure, leading to dramatic differences in mechanical properties (e.g., strength, deformation). Under impact testing, the pore ice reduces the stress concentration in the crack tips, preventing the formation of some cracks caused by compressive stress waves. For example, as saturation increases, the plastic deformation of the sample first decreases and then increases. Moreover, the enhanced phenomenon is observed in static tests, such that the strength, elastic modulus, and brittleness are usually greatly increased at low temperatures [7,32]. However, as saturation increases, the rock interior is damaged by the expansion of pore ice, weakening the strengthening effect [9]. When the two effects coexist, the saturation of the rock determines which process dominates by affecting the ice content in the pore. In other words, saturation is crucial for enhancing or damaging pore ice at low temperatures. Consequently, the influence of saturation on the mechanical properties of the samples needs further discussion.

In the dry or low-water-content frozen samples, where the internal pores are mainly occupied by air, the changes in dynamic properties during freezing are related only to the shrinkage properties of the mineral particles. As the saturation increases, the presence of pore ice becomes the main reason for the change in mechanical properties [6]. When the saturation of the sample is low, the growth of pore ice volume is limited due to the lack of pore water [37]. At this time, the pore ice in the rock has a strengthening effect, which mainly consists of three aspects: the supporting effect increases the dynamic strength or deformation resistance of the rock; the crack-filling effect reduces the stress concentration at the crack tips; and the adhesion forces between the unfrozen film water with the rock matrix and the ice improve the mechanical properties of the pore in terms of tensile and shear strength (Figure 18). When the pore water freezes into ice, the dynamic mechanical properties of the sample tend to strengthen, while the degree of fracture decreases. Moreover, the plastic deformation of the sample under dynamic compressive stress decreases with increasing saturation, which is due to the limitation of microcracks development inside the sample. However, when the saturation gradually increases (>50%), the dynamic strength of the sample decreases significantly, especially at 100% saturation. The continuous expansion of the pore ice gradually leads to the germination of microcracks in the specimens. Therefore, microcracks are more likely to develop earlier during impact loading, leading to an increase in plastic deformation (Figure 8) [1]. When saturation exceeds 50% in this work, there is sufficient water in the rock to provide a basis for the growth of frost heave during freezing. Therefore, the role of pore water in the strengthening or weakening effect needs further investigation.

As shown in Figure 18c, the pore distribution characteristics of the sample mainly include main pores, secondary pores, branch pores, and isolated pores. Since the freezing point of water in pores is inversely proportional to the pore radius, the water in the main pores freezes first and then grows into the secondary pores [27]. When the water content of the sample is low ($S_r = 30\%$), most of the unfrozen water migrates through the water film into the main pores and ice growth stops after a certain volume because there is insufficient water [25]. Consequently, the T_2 spectrum of the red sandstone in Figure 7 shows no significant change. At this time, the pore ice mainly has a strengthening effect. As saturation increases, the ice in the main pores continues to grow due to sufficient unfrozen water and drives some of the water into the secondary pores. If the pore is closed, a water pressure P_w is created in the pore. When the P_w exceeds the tensile strength of the rock skeleton, triggering the spreading of the secondary pore is the primary reason for the change in the second peak of the T_2 spectrum. When the pore is connected, the hydrostatic pressure P_i generated by the pore ice drives the unfrozen water seepage to form damage and exerts a dynamic water pressure on the rock skeleton, weakening the deformation resistance of the rock matrix [38]. The pressure P_i also provides a supporting force for the

pore wall. At the same time, the mechanical properties of ice are similar to those of rock, which reduces the wave impedance under the compressive stress wave and effectively reduces the dissipated energy. Therefore, cracks are less likely to develop in samples under impact loading due to the effect of pore ice, indicated macroscopically by an increase in the elastic phase and a decrease in the plastic deformation phase (Figure 8).

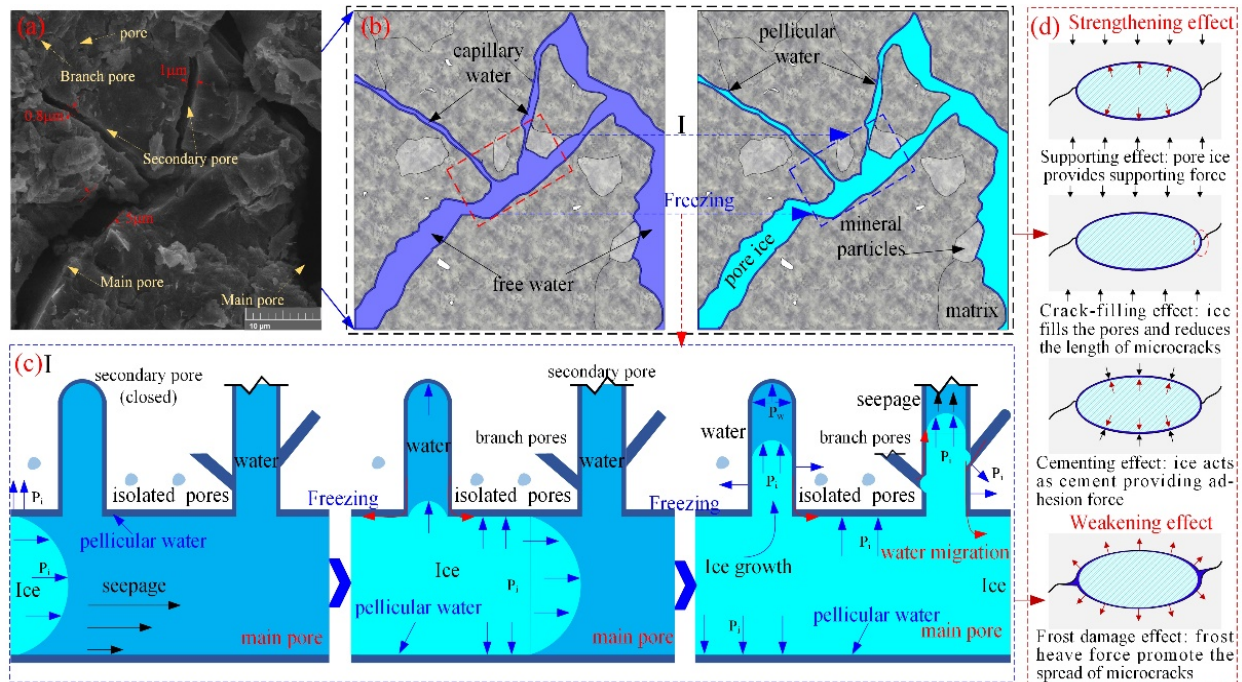


Figure 18. Expansion behavior and influence mechanism of pore ice during sandstone freezing: (a) SEM image; (b) abstracted pore structure model; (c) freezing process; (d) pore ice effects.

In addition, the ice in the main pore gradually shifts to the secondary pores during the freezing process, with the capillary mechanism playing an important role in this process [25]. Due to the relatively low chemical potential of the ice in the main pore, the supercooled water in the small pores migrates along the thin water film to the larger pores [6], resulting in a continuous growth of ice in the main pores and a gradual increase in pressure P_i . When the difference between the ice pressure P_i and the water pressure P_w is $(2\gamma_{sl}/R) \cdot \cos \theta$ (γ_{sl} is the interfacial tension between ice and water; R is the equivalent capillary radius; and θ is the contact angle [27]), the pore ice gradually develops toward the capillary pores and generates frozen expansion, which promotes the pore development. In general, the dynamic mechanical properties of frozen rock are not always enhanced with increasing saturation, with the strengthening effect suppressed when the saturation exceeds a critical value. The strengthening effect is less than the weakening effect when the saturation of the red sandstone exceeds 80%. Therefore, from the test results, the dynamic strength, modulus, and dissipated energy of the frozen sandstone gradually decrease when the saturation exceeds 80%, while the ultimate deformation capacity and broken degree progressively increase. In summary, as saturation increases, pore ice gradually transitions from filling, supporting, and bonding effects to frost damage.

5. Conclusions

The effects of saturation and impact loading on the dynamic mechanical behavior of the frozen red sandstone in the Urumqi area were investigated using a LT-SHPB system. Moreover, LT-NMR and SEM methods were employed to analyze the microstructural evolution of the frozen sandstone with different saturations. The main conclusions are as follows:

1. During freezing at low temperatures, when the saturation was below the critical saturation, the sample was dominated by the development of micropores, while meso- and macropores mainly propagated within the saturated sample, as evidenced by an increase in the second and third peaks in the T_2 spectrum of 9.32% and 3.57%, respectively. Under low temperature conditions, meso- and macropores were more sensitive to saturation and more susceptible to crystallization pressure.
2. As saturation increased, the dynamic strength, elastic modulus, and brittleness of the frozen sandstone tended to increase and then decrease. At four impact loads, the strength of the samples increased by 21.2%, 27.1%, 32.5%, and 34.3% when the saturation increased from 0% to 50%, which corresponded to 1.38, 1.43, 1.51, and 1.56 times the strength of the fully saturated samples, respectively. In addition, the dynamic mechanical properties of the frozen sandstone showed a significant effect of impact strengthening with increasing impact velocity.
3. The energy dissipation capacity of the frozen red sandstone was significantly affected by its saturation at low temperatures. When the saturation increased from dry to 50%, the energy dissipation capacity during impact gradually increased, while the energy dissipation capacity gradually decreased as saturation increased from 50% to 100%. The strengthening effect reached its maximum when the saturation of the sample was 50%. In addition, the enhancement effect of saturation on energy dissipation was smaller than the weakening effect.

Author Contributions: Methodology, J.X. and H.P.; investigation, J.X. and Z.S.; resources, J.X.; data curation, Z.S. and J.X.; writing—original draft preparation, J.X.; writing—review and editing, J.X. and H.P.; visualization, Z.S. and J.X.; supervision, H.P. All authors have read and agreed to the published version of the manuscript.

Funding: This research was funded by the National Natural Science Foundation of China (No. 51974296, No. 52061135111).

Institutional Review Board Statement: Not applicable.

Informed Consent Statement: Not applicable.

Data Availability Statement: Data available on request due to privacy restrictions.

Conflicts of Interest: The authors declare no conflict of interest.

References

1. Wang, T.; Sun, Q.; Jia, H.; Shen, Y.; Li, G. Fracture Mechanical Properties of Frozen Sandstone at Different Initial Saturation Degrees. *Rock Mech. Rock Eng.* **2022**, *55*, 3235–3252. [[CrossRef](#)]
2. Zhou, Z.; Yude, E.; Cai, X.; Zhang, J. Coupled Effects of Water and Low Temperature on Quasistatic and Dynamic Mechanical Behavior of Sandstone. *Geofluids* **2021**, *2021*, 9926063. [[CrossRef](#)]
3. Song, Y.; Yang, H.; Tan, H.; Ren, J.; Guo, X. Study on damage evolution characteristics of sandstone with different saturations in freeze-thaw environment. *Chin. J. Rock Mech. Eng.* **2021**, *40*, 1513–1524.
4. Xu, J.; Pu, H.; Sha, Z. Mechanical behavior and decay model of the sandstone in Urumqi under coupling of freeze–thaw and dynamic loading. *Bull. Eng. Geol. Environ.* **2021**, *80*, 2963–2978. [[CrossRef](#)]
5. Chen, Y.; Huidong, C.; Ming, L.; Pu, H. Study on dynamic mechanical properties and failure mechanism of saturated coal-measure sandstone in open pit mine with damage under real-time low-temperature conditions. *J. China Coal Soc.* **2022**, *47*, 1168–1179.
6. Liu, B.; Sun, Y.; Yuan, Y.; Liu, X.; Bai, X.; Fang, T. Strength characteristics of frozen sandstone with different water content and its strengthening mechanism. *J. China Univ. Min. Technol.* **2020**, *49*, 1085–1093.
7. Huang, S.; Cai, Y.; Liu, Y.; Liu, G. Experimental and Theoretical Study on Frost Deformation and Damage of Red Sandstones with Different Water Contents. *Rock Mech. Rock Eng.* **2021**, *54*, 4163–4181. [[CrossRef](#)]
8. Jia, H.; Zi, F.; Yang, G.; Li, G.; Shen, Y.; Sun, Q.; Yang, P. Influence of Pore Water (Ice) Content on the Strength and Deformability of Frozen Argillaceous Siltstone. *Rock Mech. Rock Eng.* **2020**, *53*, 967–974. [[CrossRef](#)]
9. Wang, T.; Sun, Q.; Jia, H.; Ren, J.; Luo, T. Linking the mechanical properties of frozen sandstone to phase composition of pore water measured by LF-NMR at subzero temperatures. *Bull. Eng. Geol. Environ.* **2021**, *80*, 4501–4513. [[CrossRef](#)]
10. Yamabe, T.; Neaupane, K.M. Determination of some thermo-mechanical properties of Sirahama sandstone under subzero temperature condition. *Int. J. Rock Mech. Min. Sci.* **2001**, *38*, 1029–1034. [[CrossRef](#)]

11. Kodama, J.; Goto, T.; Fujii, Y.; Hagan, P. The effects of water content, temperature and loading rate on strength and failure process of frozen rocks. *Int. J. Rock Mech. Min. Sci.* **2013**, *62*, 1–13. [[CrossRef](#)]
12. Chen, T.C.; Yeung, M.R.; Mori, N. Effect of water saturation on deterioration of welded tuff due to freeze-thaw action. *Cold Reg. Sci. Technol.* **2004**, *38*, 127–136. [[CrossRef](#)]
13. Li, J.; Kaunda, R.B.; Zhou, K. Experimental investigations on the effects of ambient freeze-thaw cycling on dynamic properties and rock pore structure deterioration of sandstone. *Cold Reg. Sci. Technol.* **2018**, *154*, 133–141. [[CrossRef](#)]
14. Zhang, J.; Deng, H.; Deng, J.; Ke, B. Development of Energy-Based Brittleness Index for Sandstone Subjected to Freeze-Thaw Cycles and Impact Loads. *IEEE Access* **2018**, *6*, 48522–48530. [[CrossRef](#)]
15. Gong, F.; Yan, J.; Luo, S.; Li, X. Investigation on the Linear Energy Storage and Dissipation Laws of Rock Materials Under Uniaxial Compression. *Rock Mech. Rock Eng.* **2019**, *52*, 4237–4255. [[CrossRef](#)]
16. Jacob, B.J.; Misra, S.; Parameswaran, V.; Mandal, N. Control of planar fabrics on the development of tensile damage zones under high-speed deformation: An experimental study with granite and gneiss. *J. Struct. Geol.* **2020**, *140*, 104418. [[CrossRef](#)]
17. Liu, X.; Liu, Y.; Dai, F.; Yan, Z. Tensile mechanical behavior and fracture characteristics of sandstone exposed to freeze-thaw treatment and dynamic loading. *Int. J. Mech. Sci.* **2022**, *226*, 107405. [[CrossRef](#)]
18. Cai, X.; Zhou, Z.; Zang, H.; Song, Z. Water saturation effects on dynamic behavior and microstructure damage of sandstone: Phenomena and mechanisms. *Eng. Geol.* **2020**, *276*, 105760. [[CrossRef](#)]
19. Song, Z.; Wang, Y.; Konietzky, H.; Cai, X. Mechanical behavior of marble exposed to freeze-thaw-fatigue loading. *Int. J. Rock Mech. Min. Sci.* **2021**, *138*, 104648. [[CrossRef](#)]
20. Yang, R.; Fang, S.; Guo, D.; Li, W.; Mi, Z. Study on Dynamic Tensile Strength of Red Sandstone Under Impact Loading and Negative Temperature. *Geotech. Geol. Eng.* **2019**, *37*, 4527–4537. [[CrossRef](#)]
21. Yang, R.; Fang, S.; Li, W.; Yang, Y.; Yue, Z. Experimental Study on the Dynamic Properties of Three Types of Rock at Negative Temperature. *Geotech. Geol. Eng.* **2019**, *37*, 455–464.
22. Zakharov, E.V. Effects of negative temperatures on crushing rocks of various deposits in Yakutia. *Obogashchenie Rud* **2021**, *2021*, 3–9.
23. Weng, L.; Wu, Z.; Liu, Q.; Wang, Z. Energy dissipation and dynamic fragmentation of dry and water-saturated siltstones under sub-zero temperatures. *Eng. Fract. Mech.* **2019**, *220*, 106659. [[CrossRef](#)]
24. Xu, J.; Pu, H.; Sha, Z. Experimental Study on the Effect of Brittleness on the Dynamic Mechanical Behaviors of the Coal Measures Sandstone. *Adv. Civ. Eng.* **2021**, *2021*, 6679333. [[CrossRef](#)]
25. Wan, Y.; Chen, G.Q.; Sun, X.; Zhang, G.Z. Triaxial creep characteristics and damage model for red sandstone subjected to freeze-thaw cycles under different water contents. *Chin. J. Geotech. Eng.* **2021**, *43*, 1463–1472.
26. Li, X. (Ed.) *Rock Dynamic Fundamentals and Applications*; Science Press: Beijing, China, 2014; ISBN 987-7-03-040425-1.
27. Cheng, H.; Chen, H.; Cao, G.; Rong, C.; Yao, Z.; Cai, H. Damage mechanism of porous rock caused by moisture migration during freeze-thaw process and experimental verification. *Chin. J. Rock Mech. Eng.* **2020**, *39*, 1739–1749.
28. Yao, Y.; Liu, D.; Che, Y.; Tang, D.; Tang, S.; Huang, W. Petrophysical characterization of coals by low-field nuclear magnetic resonance (NMR). *Fuel* **2010**, *89*, 1371–1380. [[CrossRef](#)]
29. Xing, H.Z.; Zhang, Q.B.; Ruan, D.; Dekhoda, S.; Lu, G.X.; Zhao, J. Full-field measurement and fracture characterisations of rocks under dynamic loads using high-speed three-dimensional digital image correlation. *Int. J. Impact Eng.* **2018**, *113*, 61–72. [[CrossRef](#)]
30. Dai, F.; Huang, S.; Xia, K.; Tan, Z. Some fundamental issues in dynamic compression and tension tests of rocks using split Hopkinson pressure bar. *Rock Mech. Rock Eng.* **2010**, *43*, 657–666. [[CrossRef](#)]
31. Kang, Y.; Liu, Q.; Zhao, J.; Zhang, F. Research on frost deformation characteristics of rock and simulation of tunnel frost deformation in cold region. *Chin. J. Rock Mech. Eng.* **2012**, *31*, 2518–2526.
32. Liu, B.; Sun, Y.; Han, Y.; Liu, N.; Li, T. Laboratory investigation on mechanical and hydraulic properties of sandstone under freeze-thaw cycle. *Environ. Earth Sci.* **2022**, *81*, 146. [[CrossRef](#)]
33. Liu, S.; Xu, J.; Liu, S.; Wang, P. Fractal study on the dynamic fracture of red sandstone after F-T cycles. *Environ. Earth Sci.* **2022**, *81*, 152. [[CrossRef](#)]
34. Sun, L. *Structural Evolution and Rock Pressure Activity Regularity of Weakly Cemented Strata of the Large Mining Height Work Face in Western China*; University of Science and Technology Beijing: Beijing, China, 2016; Volume 3.
35. Wu, N.; Liang, Z.Z.; Li, Y.C.; Li, H.; Li, W.R.; Zhang, M.L. Stress-dependent anisotropy index of strength and deformability of jointed rock mass: Insights from a numerical study. *Bull. Eng. Geol. Environ.* **2019**, *78*, 5905–5917. [[CrossRef](#)]
36. Zheng, G.H.; Xu, J.Y.; Wang, P.; Fang, X.Y.; Wang, P.X.; Wen, M. Physical characteristics and degradation model of stratified sandstone under freeze-thaw cycling. *Rock Soil Mech.* **2019**, *40*, 632–641.
37. Wang, B.; Sun, P.; Luo, T.; Zhang, T.; Yang, W. Freezing Pressurized Water into a Standard Cylindrical Ice Sample in a Triaxial Cell. *Geofluids* **2021**, *2021*, 6678966. [[CrossRef](#)]
38. Wu, J.; Wang, H.; Zong, Q.; Xu, Y. Experimental Investigation of Dynamic Compression Mechanical Properties of Frozen Fine Sandstone. *Adv. Civ. Eng.* **2020**, *2020*, 8824914. [[CrossRef](#)]